Published in final edited form as:
Am J Physiol Cell Physiol. 2007 November ; 293(5): C1568–C1575. doi:10.1152/ajpcell.00193.2007.

Macrorheology and adaptive microrheology of endothelial cells subjected to fluid shear stress

Jhanvi H. Dangaria and **Peter J. Butler**
Department of Bioengineering, The Pennsylvania State University, University Park, Pennsylvania

Abstract

Vascular endothelial cells (ECs) respond to temporal and spatial characteristics of hemodynamic forces by alterations in their adhesiveness to leukocytes, secretion of vasodilators, and permeability to blood-borne constituents. These physiological and pathophysiological changes are tied to adaptation of cell mechanics and mechanotransduction, the process by which cells convert forces to intracellular biochemical signals. The exact time scales of these mechanical adaptations, however, remain unknown. We used particle-tracking microrheology to study adaptive changes in intracellular mechanics in response to a step change in fluid shear stress, which simulates both rapid temporal and steady features of hemodynamic forces. Results indicate that ECs become significantly more compliant as early as 30 s after a step change in shear stress from 0 to 10 dyn/cm^2 followed by recovery of viscoelastic parameters within 4 min of shearing, even though shear stress was maintained. After ECs were sheared for 5 min, return of shear stress to 0 dyn/cm^2 in a stepwise manner did not result in any further rheological adaptation. Average vesicle displacements were used to determine time-dependent cell deformation and macrorheological parameters by fitting creep function to a linear viscoelastic liquid model. Characteristic time and magnitude for shear-induced deformation were 3 s and 50 nm, respectively. We conclude that ECs rapidly adapt their mechanical properties in response to shear stress, and we provide the first macrorheological parameters for time-dependent deformations of ECs to a physiological forcing function. Such studies provide insight into pathologies such as atherosclerosis, which may find their origins in EC mechanics.

Keywords

viscoelasticity; atherosclerosis; cell mechanics; particle tracking; mechanotransduction

The endothelium plays a primary role in vascular health and disease. As an interface between the blood and the vessel wall, it is exposed to hemodynamic forces that, in turn, influence endothelial cell-regulated vascular function. In particular, shear stress, the tangential component of hemodynamic forces, induces endothelial cells (ECs) to modulate inflammation (9), wound healing (17), hemostasis (16), vascular tone (5), and remodeling (19). Temporal and spatial characteristics of hemodynamic shear stress determine whether these responses lead to vascular health or pathologies such as atherosclerosis (4, 12). For example, rapidly changing shear with low magnitude and high spatial gradients is thought to be atherogenic (24) because it leads to increased EC permeability to low-density lipoprotein (8), increased adhesivity to monocytes (37), and increased expression of genes thought to be associated with vascular inflammation (7, 10).

Address for reprint requests and other correspondence: P. J. Butler, Dept. of Bioengineering, The Pennsylvania State University, 228 Hallowell Building, University Park, PA 16802 (pbutler@psu.edu).

Although the precise molecular mechanisms of mechanotransduction remain the focus of many studies, there is an increasing effort to characterize mechanical properties of ECs and to incorporate these properties into predictive mechanical models to characterize cellular responses to external forces (6, 15, 22, 29). While these models tend to use static mechanical properties, adaptive changes in mechanical properties are particularly relevant because it is possible that mechanical adaptation is related to whether ECs exhibit a physiological or pathophysiological phenotype. For example, using the micropipette aspiration technique, Sato et al. (34) reported that porcine aortic ECs exposed to 24 h of fluid shear exhibited a twofold increase in elasticity and a threefold increase in viscosity compared with nonsheared counterparts. In a similar study where atomic force microscopy (AFM) was used on ECs, a significant increase in Young's modulus was reported after 6 h of exposure to shear stress compared with preshear values (32). Lee et al. (26) used particle-tracking microrheology to demonstrate a Rho-kinase-dependent stiffening of the fibro-blast cytoplasm 40 min after the onset of shear stress. Together, these studies suggest that ECs undergo adaptations in their rheological properties in response to fluid shear stress on the time scale of hours. It is not yet clear, however, whether shear-mediated changes in EC mechanics on the time scale of seconds to minutes exist. These time scales are important because they are equivalent to the time scales of temporal changes in shear stress during the cardiac cycle and during rapid changes in vascular load resulting from exercise.

Although cells change their mechanical properties in response to extracellular chemical and mechanical stimuli, there exists a need for mathematical models by which cell deformations in response to force are predicted through the use of time-independent mechanical constants. Provided that these models are used for time scales shorter than those governing adaptive changes, these models can be invaluable in computational methods in mechanobiology (6, 15, 22). AFM and micropipette aspiration can characterize mechanical properties of cells, but these methods use forces that are different from shear stress in magnitude and direction, leading to bulk rheological constants that may be inappropriate for models that characterize the time-dependent EC deformation and intracellular stresses in response to fluid flow.

Thus we designed experiments to test whether shear induces rapid changes in EC rheology and determined bulk rheological properties, which characterize time-dependent deformation of ECs due to shear stress. Multiple particle-tracking microrheology (38) was used to determine the evolution of cytoplasmic microrheological parameters in response to a step change in shear stress, and the bulk motion of embedded endogenous vesicles was converted to shear strain and fit with the analytical solution to the creep response of the cytoplasm using a phenomenological model of a linear viscoelastic liquid. Such studies establish the earliest measured time scale of EC mechanoadaptation, which is adaptation of EC mechanical properties, and provide the first rheological constants for mechanical models of ECs measured using shear stress as the forcing function.

MATERIALS AND METHODS

Cell culture

Bovine aortic ECs (VEC, Rensselaer, NY) were cultured in MCDB-131 complete medium supplemented with 11% fetal bovine serum (FBS), 100 U/ml penicillin, and 100 μg/ml streptomycin. Cells between *passages 3* and *10* were initially subcultured in T-25 flasks, maintained at 37°C in a humidified environment with 5% CO_2, and later grown to ~90% confluence on 40-mm circular, no. 1 glass coverslips.

Flow chambers, vibration control, and imaging system

To maintain the physiological environment during imaging, coverslips with cell monolayers were assembled in a parallel-plate flow chamber [Focht Chamber System (FCS2), Bioptechs, Butler, PA]. The flow chamber was then mounted on a piezo-controlled microscope stage (Nano-View/M, Mad City Labs, Madison, WI) with a manual two-axis coarse-positioning system and a locking feature to prevent long-term stage drift. These methods of ensuring mechanical stability were essential features in accurate nanoscale tracking measurements.

The flow-loop system consisted of four media reservoirs connected through a computer-controlled, six-port modular valve positioner (MVP) (Hamilton, Reno, NV) such that at a time only two reservoirs were connected to the flow chamber. Through this system, the MVP could switch between upstream and downstream reservoirs that had equal pressures or ones that induced a pressure gradient. This setup resulted in a step change in shear stress from 0 to 10 dyn/cm^2 with negligible pressure changes inside the flow chamber (and negligible attendant coverslip deflection). To correlate cell deformations with time-dependent stresses, pressure changes across the flow chamber were continuously monitored using a differential pressure transducer (model DP-15, Validyne Engineering, Northridge, CA). Dulbecco's modified Eagle's medium supplemented with 10% FBS (GIBCO, Carlsbad, CA) was used as the perfusion medium. pH was maintained by using superfusion of 5% CO_2 over the media reservoirs.

Cells were imaged under differential interference contrast (DIC) microscopy using an Olympus IX71 inverted research microscope with a ×60 Plan Apo oil-immersion objective [1.45 numerical aperture (NA)]. To further improve the resolution in the DIC mode, a ×60 LUMPlanFL water-immersion objective (0.90 NA) was used in place of the condenser, and an immersion oil with a refractive index of 1.33 (series AAA, Cargille Laboratories) was used in place of water to prevent evaporation of immersion medium. Time-lapse images were acquired by a high-resolution, 12-bit charge-coupled device camera, Sensicam QE (Cooke), at 20–30 frames per second with exposure times of 1–3 ms with an image resolution of 0.1 μm/pixel.

Experimental protocols

To study shear-induced variations in cell microrheology, ECs were exposed to a step change in fluid shear stress of 10 dyn/cm^2, which was held constant for a total of 5 min. Continuous imaging was employed over time spans of up to 90 s (limited by computer memory) to capture steady-state vesicle motion before, during, and after shear and temporal characteristics of the responses of the cell to a step shear from 0 to 10 dyn/cm^2 or from 10 to 0 dyn/cm^2. The exact temporal characteristics of the step were evaluated by fitting the shear-vs.-time waveform to a sigmoidal curve. The half-maximal shear was obtained at 0.36 s, which was an order of magnitude shorter than the time-constant governing cell deformation. Endogenous vesicles were tracked in a focal plane 2–4 μm (average of 3 μm) from the base of each cell. Two-dimensional trajectories of endogenous vesicles were calculated before step flow was imposed (preshear) (Fig. 1*B*), 30 s and 4 min after onset of flow (during shear) (Fig. 1, *C* and *D*), and 30 s after returning flow to 0 dyn/cm^2 in a stepwise manner (postshear) (Fig. 1*E*). In each case, data were collected for 30 s during a period where cell deformation was minimal. Control experiments in which flow was delivered through the chamber without cells demonstrated that flow imposition did not induce system vibration. Use of fiduciary markers during shear stress application is an alternative way to address artifacts due to system vibration (11).

Particle-tracking microrheology

Two-dimensional trajectories of endogenous vesicles in ECs were measured using an intensity-weighted, centroid-based particle-tracking algorithm custom written in LabVIEW 7.0 (National Instruments, Austin, TX). To measure intracellular mechanics, particle-tracking data of endogenous vesicles in each cell were pooled. Random displacements of vesicles over 30 s were then converted to time-averaged mean square displacements (MSD)

$$\langle \Delta r^2(\tau) \rangle$$

for various lag times τ as follows:

$$\langle \Delta r^2(\tau) \rangle = \langle [x(t+\tau) - x(t)]^2 \rangle + \langle [y(t+\tau) - y(t)]^2 \rangle \quad (1)$$

Creep compliance, (τ), was related to the ensemble-averaged MSD by:Downloaded from

$$\Gamma(\tau) = \frac{3\pi a}{2k_B T} \langle \Delta r^2(\tau) \rangle \quad (2)$$

This equation describes the local deformation of the cytoplasm by the thermally driven tracer motions (42). The factor 3/2 accounts for tracking two-dimensional projections of three-dimensional displacements (23). Frequency-dependent viscoelastic moduli of the EC cytoplasm were also calculated from MSD using the generalized Stokes-Einstein relation (27, 28):

$$G^*(\omega) = G'(\omega) + iG''(\omega) = \frac{k_B T}{\pi a i \omega \, \mathcal{F}\{\langle \Delta r^2(\tau) \rangle\}} \quad (3)$$

where $G^*(\omega)$ is the complex shear modulus, k_B is Boltzmann's constant, T is temperature (Kelvin), a is the vesicle radius, i is $\sqrt{(-1)}$, and

$$\mathcal{F}\{\langle \Delta r^2(\tau) \rangle\}$$

is the Fourier transform of the MSD. The elastic (storage) modulus $G'(\omega)$ and viscous (loss) modulus $G'(\omega)$ are the real and imaginary components of the complex shear modulus. The phase angle $\delta(\omega)$ is an indication of the solid-like ($\delta = 0°$) or liquid-like ($\delta = 90°$) behavior (43) of the medium.

$$\delta(\omega) = \tan^{-1}\left[\frac{G''(\omega)}{G'(\omega)}\right] \quad (4)$$

Ensemble-averaged MSDs of at least eight vesicles in each cell were used to compute the rheological parameters. Bovine aortic ECs have very limited endogenous vesicles, thus

precluding detection of regional variations of EC mechanical properties. Hence, G' (ω) and G'' (ω) were calculated from average MSD of all vesicles in a given cell. Compliance, elastic, and shear moduli were averaged across multiple cells (n = 6) and reported as means ± SE.

Using shear stress and bulk deformation to determine macrorheology

To study the macroscale viscoelasticity (or macrorheology) of ECs, the creep function $J(t)$ (Eq. 5) for a phenomenological model consisting of springs and dashpots was fit to the average creep response. Creep response is the average time-dependent shear strain in response to step shear of 10 dyn/cm^2. The shear strain is the average displacement of all vesicles divided by the height (3 μm) of the vesicles above the coverslip. All vesicle displacements were computed as relative to their location at the instant step shear was initiated or removed. The creep compliance for the model shown in Fig. 4*C* that relates shear strain to a step change in shear stress is given by:

$$J(t)=\frac{\gamma(t)}{\sigma_0}=\frac{1}{\mu_v}(1-e^{-t/\tau_v})+\frac{1}{\eta_s}t \tag{5}$$

where $\gamma(t)$ is the shear strain, σ_0 is the shear stress, and μ_v and η_v are the elastic and viscous moduli of the Voigt body, respectively;

$$\tau_v=\frac{\eta_v}{\mu_v}$$

is the relaxation time, and η_s is the viscosity of the dashpot in series with the Voigt body.

Data analysis and statistics

Compliance and shear moduli were expressed as means ± SE. Significance of shear-induced changes in compliance and shear moduli with respect to preshear values were assessed using repeated measures ANOVA applied at selected time lags and frequencies with $P < 0.05$ indicating significance. For macrorheology, time-dependent vesicle displacements (as indices of shear deformations) were plotted, and displacements at selected time points were expressed as means ± SD to illustrate cell-to-cell variation. Confidence intervals (95%) were computed, and displacements were considered significant if confidence intervals did not include 0 (no displacement). The average displacement curve was converted to creep compliance as described in MATERIALS AND METHODS and curve fit with the model for a viscoelastic liquid (Eq. 5). All curve fitting was performed using Origin 7.5 (OriginLab, Northampton, MA), and statistical analysis was performed using SAS (SAS Institute, Cary, NC).

RESULTS

Shear stress induces an increase in MSD of endogenous vesicles

Vesicle trajectories were converted into ensemble-averaged MSD plotted against increasing lag times. Overall, the MSD curves exhibited power-law scaling

$$\langle \Delta r^2(\tau) \rangle \sim \tau^{\alpha}$$

where $\alpha < 1$ indicates subdiffusive behavior (35). When step shear stress was applied, MSD evaluated at 30 s after step shear increased for all time lags (Fig. 2*A*). MSD returned to control values at 4 min despite the maintenance of shear stress and remained the same after cessation of shear stress. Furthermore, there was no change in the *x*, *y* distribution of vesicle trajectories, indicating that MSDs were not skewed by cell deformation. MSDs were converted to creep compliance using Eq. 2. Creep compliance increased twofold over static conditions as early as 30 s after shear stimulation (Fig. 2*B*). This increase was significant and consistent for all lag times greater than 1 s. A 1.5-fold increase in mean cellular compliance was observed after 4 min of shear, although this increase was not found to be significant, which suggests that cell compliance returned to control values after 4 min of shearing. Stimulating cells with stepwise removal of shear stress did not influence EC mechanical properties. Thus ECs respond rapidly and transiently to applied step change in shear stress by softening their cytoplasm.

Shear induces changes in microrheology

To characterize the intracellular mechanics of ECs, frequency-dependent viscoelastic moduli $G'(\omega)$ and $G''(\omega)$ were calculated from the ensemble-averaged MSD, where the frequency ω is the inverse of time lag τ The entire frequency spectrum was plotted to highlight the frequency-dependent nature of shear effects on viscoelastic moduli. Thirty seconds after onset of step flow a significant decrease ($P < 0.05$) in $G'(\omega)$ at all frequencies and $G''(\omega)$ at all frequencies $\leq 1\ s^{-1}$ compared with preshear values was observed (Fig. 3, *A* and *B*). After 4 min of exposure to shear stress, $G'(\omega)$ and $G''(\omega)$ returned to control values, and no additional modulation of microrheology was observed in response to step change in shear stress from 10 to 0 dyn/cm^2. Thus ECs exhibit time-varying, frequency-dependent changes in microrheological properties in response to step changes in fluid shear stress.

Plots of phase angles suggest that at lower frequencies ($\omega < 1\ s^{-1}$), EC cytoplasm behaved like a viscoelastic liquid while a solid-like behavior was observed at higher frequencies ($\omega > 1\ s^{-1}$) (Fig. 3*C*). After onset of step shear stress (30 s), the crossover frequency (i.e., frequency at which $\delta = 45°$) increased from the control value $\omega = 1\ s^{-1}$ to $\omega = s^{-1}$ (i.e., the EC cytoplasm behaved more liquid-like compared with pre-shear conditions). After shear was turned off, even though crossover frequency was comparable with preshear, ECs exhibited lower phase angles and, thus, a dominant elastic nature.

Shear induces viscoelastic fluid-like deformation

Global cell deformation was determined from average vesicle displacements at the moment of shear onset and is shown in Fig. 4, *A* and *B*. When individual cell responses were analyzed, it was noted that the deformation was highly heterogeneous (indicated by large standard deviations) with some cells deforming rapidly and dramatically and others exhibiting little or no deformation. On average, ECs exhibited a rapid deformation on the order of 50 nm in the direction of shear stress. The initial phase of rapid deformation is seen within seconds while a slow gradual rise is observed soon after shear stress peaked (Fig. 4*A*). Deformation in the orthogonal (*x*) direction was negligible for all instances. After cells were sheared for 5 min, shear was returned to 0 dyn/cm^2 in a stepwise fashion. Cells showed negligible average deformation in response to the removal of shear stress, although standard deviations of deformations were reduced upon shear removal (Fig. 4*B*).

To examine the macroscale EC mechanical properties, average creep response was plotted as a function of time after the onset of step change in shear stress (Fig. 4*C*). Global cell mechanics was characterized by fitting the average creep response relating shear stress to shear strain using a phenomenological Voigt-Maxwell model of springs and dashpots (Fig. 4*C*, *inset*) (14). The initial rapid response correlated with the onset of step shear and was

accounted for by the solid-like behavior described by the Voigt body while the liquid-like behavior at long times was accounted for by the series dashpot. Average macrorheological properties were calculated to be as follows: shear modulus, μ_v = 60.6 Pa; viscosities, η_v = 183.65 Pa•s, η_s = 5,000 Pa•s; and relaxation time, τ_v = 3.03 s. τ_v is the effective relaxation time of the voigt body, which reflects the time required to establish initial elastic stresses and flow;

$$\tau_s = \frac{\eta_s}{\mu_v}$$

describes the effective relaxation time of the Voigt-Maxwell model describing long-term viscous flow and was calculated to be τ_s = 83 s.

DISCUSSION

The main findings of this study are described as follows. First, shear stress was found to induce an increase in cellular compliance and corresponding changes in microrheological moduli as early as 30 s after shear onset, as measured by particle-tracking microrheology. Second, shear stress elicited heterogeneous viscoelastic deformations that could be well described using the linear viscoelasticity theory with a length scale of 50 nm and two time scales: a viscoelastic solid-like deformation with a time scale of 3 s and a long-term viscoelas-tic fluid-like deformation with a time scale of 83 s. Such results provide insight into adaptive rheology of ECs and provide the first quantitative measurements of macrorheology relevant to shear-induced deformation.

Shear-induced adaptive microrheology

We report for the first time that ECs respond to shear stress at very early time points (on the order of seconds) by softening, i.e., reducing their elasticity and viscosity. Mechanical properties recovered during 4 min of exposure to shear stress, and no additional change was observed after shear was turned off, indicating that cells remodeled during exposure to shear to reach a new mechanical state. Consistent with this observation, in a study on neutrophils, Yap and Kamm (45) reported a drop in shear moduli within seconds after mechanical stimulation, suggesting a sudden cytoskeleton disruption. In contrast, Lee et al. (26) demonstrated a Rho-kinase-dependent stiffening of the fibroblast cytoplasm 40 min after the onset of shear stress. It is possible that these apparent contradictions can be reconciled by noting that cells may soften at early time points followed by stiffening at later time points. In other words, adaptation of cells may be sensitive to the duration of exposure to shear stress. Although the exact mechanisms of adaptive rheology were beyond the scope of our study, it is possible that these early shear-mediated effects were due to rapid deformation or turnover in the cytoskeleton. With respect to deformation, Helmke et al. (20) reported intermediate filament displacements minutes after the onset of fluid flow. An increase in actin-filament turnover and net depolymerization of the actin cytoskeleton due to fluid shear stress within 5 min of shear exposure was observed by Osborn et al. (33). Rho GTPases have been implicated in shear-mediated cytoskeletal remodeling in which shear stress triggers a decrease in Rho activity after 5 min of exposure (39). Reductions in Rho activity have been implicated in depolymerization of actin. Furthermore, shear stress elicits an increase in G-actin content in ECs due to actin depolymerization through Ca^{2+} and PKC-dependent pathways (31). Taken together, these studies and ours support the idea that the time scales of deformation and remodeling of the cytoskeleton in response to shear stress may be complementary.

While the use of particle tracking to determine microrheology is widespread, there exists controversy regarding the molecular underpinnings of constrained motion of endogenous particles. In our study we tracked the same vesicles before and after shear stress and determined changes in rheological parameters by average MSDs of multiple vesicles on a cell-by-cell basis. Thus, although the magnitudes of microrheological parameters should be considered effective values, the changes in MSD and resulting microrheology due to shear stress are substantial and significant. Nevertheless, microrheological evidence of elastic behavior at high frequencies and viscous behavior at low frequencies agrees well with the macrorheological model of a viscoelastic liquid. Quantitative differences between internal microrheological measurements (obtained from particle tracking) and surface rheological measurements [e.g., atomic force microscopy (1), magnetic-twisting cytometry (41), and laser-tracking rheology (43)] have recently been reported and support a mechanical model for ECs of a stiff cortical shell surrounding a softer cytoplasm (21). Consistent with this model, our cytoplasmic measurements of $G'(\omega)$ and $G''(\omega)$ ranged from 0.1 to 10 Pa. These values are lower than surface measurements obtained using AFM for alveolar and bronchial lung epithelial cells in which $G'(\omega)$ ranged from 400 to 2,000 Pa and $G''(\omega)$ ranged from 100 to 3,000 Pa over frequencies of 0.1–100 Hz (1). Using laser-tracking microrheology of endogenous granules, Yamada et al. (43) reported differences in shear moduli around the nucleus and in the lamella, with the lamella being stiffer (thin lamella are sensitive to cortical actin rheology). Values ranged from 10 to 1,000 Pa. Yanai et al. (44) optically trapped intracellular granules in neutrophils and computed viscoelastic parameters from measured granular displacements after step changes in trap position. Similar to our results, intracellular stiffness values were reported on the order of 0.7 to 7 Pa. Taken together, these results suggest that the cytoplasm is softer than the cortical actin membrane shell. Thus our detection of shear-induced increases in compliance from particle tracking of intracellular endogenous organelles should be interpreted as shear-induced softening of the EC cytoplasm. Shear-induced changes in the cortical cytoskeleton remain a topic of further investigations.

Measurements of macrorheology using shear-induced organelle displacement

Various techniques have been used to determine cell macrorheology including micropipette aspiration (34, 36), AFM (32), and magnetic bead microrheometry (2). Using the micropipette aspiration technique, Sato et al. (34) reported values of elastic constants on the order of 100–300 Pa, whereas viscosity and relaxation time were on the order of 10 kPa-s and 100–200 s, respectively. Elastic moduli for static and sheared cells obtained by AFM were 0.87 and 1.75 kPa, respectively (32). Similarly, using magnetic bead microrheometry on fibroblasts, Bausch et al. (2) reported average shear modulus and viscosity to be 20–40 kPa and 2,000 Pa•s, respectively. Compared with magnitude of shear forces on the order of 300 Pa in the magnetic bead microrheometry technique, values reported in this study are on the order of 1 Pa. While the shear modulus is orders of magnitude higher than our reported value of 60 Pa, the effective viscosity is comparable with our value of 5,000 Pa•s.

Although the elastic moduli obtained by micropipette aspiration were similar to those obtained in our study on macrorheology, the effective macrorheological elastic constants, viscosities, and relaxation times obtained in our study by tracking average motion of endogenous organelles in response to step shear are an order of magnitude lower than those obtained by the techniques used in our study. Discrepancies in macrorheological constants may arise from factors including differences in the nature and magnitude of applied force (e.g., shear stress vs. twisting), the region where the cell is probed (e.g., surface or in the interior of cell), and cell type. In our study, macrorheological parameters were measured from small-scale deformations on the order of 50 nm in response to step changes in shear stress. It is likely that the large deformations used in AFM and micropipette aspiration result

in different measured viscoelastic moduli than those resulting from small displacements induced by physiological shear stress. Second, AFM indents the cell normal to the surface while shear stress is tangential. Mechanical anisotropy of the cell would result in force-direction-dependent moduli. Third, micropipette aspiration measures mechanical constants of cells detached from their substrate. Detachment may affect the effective mechanical properties of cells. Fourth, discrepancies in moduli may also arise from the fact that both AFM and micropipette aspiration techniques probe the cell externally, whereas deformation of endogenous probes yields trajectories that arise from surface deformation transmitted to the interior. In conclusion, the use of shear stress as a forcing function and interior organelle tracking to assess deformation yields viscoelastic moduli that have direct application to models of sheared endothelium while avoiding inherent assumptions used in other mechanical techniques.

In this study, we characterized the EC viscoelasticity in terms of a simple mechanical circuit consisting of elementary springs and dashpots. The response of ECs to a step change in shear stress was described by a Voigt-Maxwell model. The Voigt element consisted of a parallel arrangement of a spring and dashpot and accounted for the solid-like behavior at short times, whereas a dashpot in series was responsible for the liquid-like behavior at long times. The relaxation time τ_v governed the initial viscous flow regime. After time τ_v, the EC cytoplasm behaved like a viscoelastic liquid with viscosity η_s. The rapid short time-scale response could be due to moderately elastic cortical cytoskeleton while the longer and more viscous response could be due to the deep cytoskeleton component (25). This conclusion is consistent with the elastic behavior of the cell during rapidly changing shear stress and microrheological determination of solid-like behavior at high frequencies, whereas, at low frequencies (e.g., steady shear), the cell behaved as a viscoelastic liquid (see Fig. 3*C*).

Modeling ECs as viscoelastic liquids has an inherent limitation in that it cannot account for adaptive changes in rheological constants. In our study, at the 5-min time point, ECs did not exhibit any elastic recoil when shear stress was turned off in a stepwise manner, thus indicating cell adaptation to shear stress on the time scale of a few minutes. Even though the macrorheology model does not explain this long-term adaptation, it nonetheless represents an important advancement in EC mechanics by providing mechanical constants for models of early (seconds) time-dependent cell deformation in response to shear stress.

Ferko et al. (15) recently developed a multicomponent-continuum elastic model for sheared and focally adhered ECs that, despite its simplicity in ascribing all mechanics to organelle-dependent elastic constants, was capable of predicting experimentally observed deformation in response to physiologically (e.g., shear stress) and experimentally- (magnetic bead) relevant mechanical stimuli (15). The magnitude of overall EC deformation in the direction of shear stress was on the order of 50 nm, which is consistent with the results reported in this study. The Ferko model could be improved through the use of elastic and viscous moduli determined from physiological forcing functions and measured time-dependent cell deformations. Together, assessment of macrorheological constants along with adaptive microrheology would elucidate the transient nature of cell mechanics while providing input into a viscoelastic model with predictive value.

Heterogeneity in individual cell deformations was observed, which may indicate heterogeneous responses to mechanical stimuli. If the time dependence of deformation in response to shear stress is different from cell to cell, this could set up stresses between cells, leading to mechanotransduction events (13, 30, 40). In a similar argument, variations in shear stress from cell to cell may induce gradations in cell deformation resulting in intercellular junctional stresses (M. H. Friedman, personal communication). Also, the time-varying mechanical properties may be related to increased lipid diffusion, as studied

previously by Butler et al. (3). Shear-mediated softening response may lead to increased deformation and membrane stresses leading to increases in lipid diffusion (18).

EC cytoskeleton and cell mechanics

Although molecular mechanisms of mechanotransduction remain at the center of controversy, growing evidence points toward a greater role of the EC actin cytoskeleton in transmission and intracellular distribution of shear forces from the apical cell surface. In vivo, actin filaments are associated into a complex, prestressed network of bundles cross-linked by proteins such as α-actinin and filamin, which, together, provide a mechanical framework to sustain cell shape, motility, and mechanosensitivity. To better understand the role of the cytoskeleton in modulating cell mechanics and shear-mediated responses, it may be necessary to study the underlying origin of the viscoelasticity of the cytoskeleton network and its associated components as a whole. The current results showing a softening of the cell cytoplasm in response to shear stress suggest that shear stress may initiate signaling pathways leading to rapid changes in actin prestress, bundling, cross-linking, or polymerization state.

Shear-induced macrorheology and adaptive microrheology in ECs

In this study, shear-induced deformations and adaptive rheology have been demonstrated to occur on time scales close to those governing rate-sensitive responses of ECs, suggesting that EC rate sensitivity (4, 5) to shear stress may find its origins in cell viscoelasticity. Furthermore, the phenomenological model for macrorheology does not distinguish between passive and active mechanisms of time-dependent deformation. Therefore, viscous dissipation in the macrorheological model may, in part, be due to adaptive microrheology. While our microrheological and macrorheological data support the concept that cells are solid at high rates of force application and liquid at lower rates, further research is necessary to precisely determine the molecular origins of microrheology, macrorheology, and their connections. Macrorheological parameters measured here will also be helpful in the development of cell-specific mechanical models that predict time-dependent stress distributions in subcellular locations (15). Together, the present studies on adaptive microrheology and macrorheology support an emerging paradigm in cell mechanics in which mechanical parameters adapt to the prevailing force. Thus adaptive rheology may be an important parameter in cellular mechanotransduction and vascular mechanobiology.

Acknowledgments

GRANTS

This work was supported in part by grants from National Heart, Lung, and Blood Institute Grant R01 HL-07754201A1 and National Science Foundation Career Award BES-0238910 (to P. J. Butler).

References

1. Alcaraz J, Buscemi L, Grabulosa M, Trepat X, Fabry B, Farre R, Navajas D. Microrheology of human lung epithelial cells measured by atomic force microscopy. Biophys J. 2003; 84:2071–2079. [PubMed: 12609908]
2. Bausch AR, Ziemann F, Boulbitch AA, Jacobson K, Sackmann E. Local measurements of viscoelastic parameters of adherent cell surfaces by magnetic bead microrheometry. Biophys J. 1998; 75:2038–2049. [PubMed: 9746546]
3. Butler PJ, Norwich G, Weinbaum S, Chien S. Shear stress induces a time- and position-dependent increase in endothelial cell membrane fluidity. Am J Physiol Cell Physiol. 2001; 280:C962–C969. [PubMed: 11245613]

4. Butler PJ, Tsou TC, Li JYS, Usami S, Chien S. Rate sensitivity of shear-induced changes in the lateral diffusion of endothelial cell membrane lipids: a role for membrane perturbation in shear-induced MAPK activation. FASEB J. 2002; 16:216–218. [PubMed: 11744620]
5. Butler PJ, Weinbaum S, Chien S, Lemons DE. Endothelium-dependent, shear-induced vasodilation is rate-sensitive. Microcirculation. 2000; 7:53–65. [PubMed: 10708337]
6. Charras GT, Horton MA. Determination of cellular strains by combined atomic force microscopy and finite element modeling. Biophys J. 2002; 83:858–879. [PubMed: 12124270]
7. Chen BPC, Li YS, Zhao Y, Chen KD, Li S, Lao J, Yuan S, Shyy JYJ, Chien S. DNA microarray analysis of gene expression in endothelial cells in response to 24-h shear stress. Physiol Genomics. 2001; 7:55–63. [PubMed: 11595792]
8. Chien S. Molecular and mechanical bases of focal lipid accumulation in arterial wall. Prog Biophys Mol Biol. 2003; 83:131–151. [PubMed: 12865076]
9. Chiu JJ, Chen LJ, Chang SF, Lee PL, Lee CI, Tsai MC, Lee DY, Hsieh HP, Usami S, Chien S. Shear stress inhibits smooth muscle cell-induced inflammatory gene expression in endothelial cells: role of NF-κB. Arterioscler Thromb Vasc Biol. 2005; 25:963–969. [PubMed: 15718492]
10. Dai G, Kaazempur-Mofrad MR, Natarajan S, Zhang Y, Vaughn S, Blackman BR, Kamm RD, Garcia-Cardena G, Gimbrone MA Jr. Distinct endothelial phenotypes evoked by arterial waveforms derived from atherosclerosis-susceptible and resistant regions of human vasculature. Proc Natl Acad Sci USA. 2004; 101:14871–14876. [PubMed: 15466704]
11. Dangaria JH, Yang S, Butler PJ. Improved nanometer-scale particle tracking in optical microscopy using microfabricated fiduciary posts. Biotechniques. 2007; 42:437–440. [PubMed: 17489228]
12. Davies PF, Barbee KA, Lal R, Robotewskyj A, Griem ML. Hemo-dynamics and atherogenesis. Endothelial surface dynamics in flow signal transduction. Ann NY Acad Sci. 1995; 748:86–102. [PubMed: 7695226]
13. DePaola N, Davies PF, Pritchard WF Jr, Florez L, Harbeck N, Polacek DC. Spatial and temporal regulation of gap junction connexin43 in vascular endothelial cells exposed to controlled disturbed flows in vitro. Proc Natl Acad Sci USA. 1999; 96:3154–3159. [PubMed: 10077653]
14. Feneberg W, Westphal M, Sackmann E. Dictyostelium cells' cytoplasm as an active viscoplastic body. Eur Biophys J. 2001; 30:284–294. [PubMed: 11548131]
15. Ferko MC, Bhatnagar A, Garcia MB, Butler PJ. Finite-element stress analysis of a multicomponent model of sheared and focally-adhered endothelial cells. Ann Biomed Eng. 2007; 35:208–223. [PubMed: 17160699]
15a. Lamack JA, Friedman MH. Individual and combined effects of shear stress magnitude and spatial gradient on endothelial cell gene expression. Am J Physiol Heart Circ Physiol. 10.1152/ajpheart.00244.2007
16. Galbusera M, Zoja C, Donadelli R, Paris S, Morigi M, Benigni A, Figliuzzi M, Remuzzi G, Remuzzi A. Fluid shear stress modulates von Willebrand factor release from human vascular endothelium. Blood. 1997; 90:1558–1564. [PubMed: 9269774]
17. Gojova A, Barakat AI. Vascular endothelial wound closure under shear stress: role of membrane fluidity and flow-sensitive ion channels. J Appl Physiol. 2005; 98:2355–2362. [PubMed: 15705727]
18. Gov NS. Diffusion in curved fluid membranes. Physiol Rev E Stat, Nonlin, Soft Matter Phys. 2006; 73:0419186.
19. Gusic RJ, Myung R, Petko M, Gaynor JW, Gooch KJ. Shear stress and pressure modulate saphenous vein remodeling ex vivo. Biomechan. 2005; 38:1760–1769.
20. Helmke BP, Thakker DB, Goldman RD, Davies PF. Spatiotemporal analysis of flow-induced intermediate filament displacement in living endothelial cells. Biophys J. 2001; 80:184–194. [PubMed: 11159394]
21. Hoffman BD, Massiera G, Van Citters KM, Crocker JC. The consensus mechanics of cultured mammalian cells. Proc Natl Acad Sci USA. 2006; 103:10259–10264. [PubMed: 16793927]
22. Karcher H, Lammerding J, Huang H, Lee RT, Kamm RD, Kaazempur-Mofrad MR. A three-dimensional viscoelastic model for cell deformation with experimental verification. Biophys J. 2003; 85:3336–3349. [PubMed: 14581235]

23. Kole TP, Tseng Y, Jiang I, Katz JL, Wirtz D. Intracellular mechanics of migrating fibroblasts. Mol Biol Cell. 2005; 16:328–338. [PubMed: 15483053]
24. Ku DN, Giddens DP, Zarins CK, Glagov S. Pulsatile flow and atherosclerosis in the human carotid bifurcation. Positive correlation between plaque location and low oscillating shear stress. Arterioscler Thromb Vasc Biol. 1985; 5:293–302.
25. Laurent VM, Fodil R, Canadas P, Fereol S, Louis B, Planus E, Isabey D. Partitioning of cortical and deep cytoskeleton responses from transient magnetic bead twisting. Ann Biomed Eng. 2003; 31:1263–1278. [PubMed: 14649500]
26. Lee JSH, Panorchan P, Hale CM, Khatau SB, Kole TP, Tseng Y, Wirtz D. Ballistic intracellular nanorheology reveals ROCK-hard cytoplasmic stiffening response to fluid flow. J Cell Sci. 2006; 119:1760–1768. [PubMed: 16636071]
27. Mason TG, Ganesan K, van Zanten JH, Wirtz D, Kuo SC. Particle tracking microrheology of complex fluids. Physiol Rev Lett. 1997; 79:3282–3285.
28. Mason TG. Estimating the viscoelastic moduli of complex fluids using the generalized Stokes-Einstein equation. Rheologica Acta. 2000; 39:371–378.
29. Mazzag BM, Tamaresis JS, Barakat AI. A model for shear stress sensing and transmission in vascular endothelial cells. Biophys J. 2003; 84:4087–4101. [PubMed: 12770912]
30. Miao H, Hu YL, Shiu YT, Yuan S, Zhao Y, Kaunas R, Wang Y, Jin G, Usami S, Chien S. Effects of flow patterns on the localization and expression of VE-cadherin at vascular endothelial cell junctions: in vivo and in vitro investigations. Vasc Res. 2005; 42:77–89.
31. Morita T, Kurihara H, Maemura K, Yoshizumi M, Nagai R, Yazaki Y. Role of Ca^{2+} and protein kinase C in shear stress-induced actin depolymerization and endothelin 1 gene expression. Circ Res. 1994; 75:630–636. [PubMed: 7923609]
32. Ohashi T, Ishii Y, Ishikawa Y, Matsumoto T, Sato M. Experimental and numerical analyses of local mechanical properties measured by atomic force microscopy for sheared endothelial cells. Biomed Mater Eng. 2002; 12:319–327. [PubMed: 12446947]
33. Osborn EA, Rabodzey A, Dewey CF Jr, Hartwig JH. Endothelial actin cytoskeleton remodeling during mechanostimulation with fluid shear stress. Am J Physiol Cell Physiol. 2006; 290:C444–C452. [PubMed: 16176968]
34. Sato M, Ohshima N, Nerem RM. Viscoelastic properties of cultured porcine aortic endothelial cells exposed to shear stress. Biomechan. 1996; 29:461–467.
35. Saxton MJ, Jacobson K. Single-particle tracking: applications to membrane dynamics. Annu Rev Biophys Biomol Struct. 1997; 26:373–399. [PubMed: 9241424]
36. Schmid-Schonbein GW, Sung KL, Tozeren H, Skalak R, Chien S. Passive mechanical properties of human leukocytes. Biophys J. 1981; 36:243–256. [PubMed: 6793106]
37. Tsao PS, Buitrago R, Chan JR, Cooke JP. Fluid flow inhibits endothelial adhesiveness: nitric oxide and transcriptional regulation of VCAM-1. Circulation. 1996; 94:1682–1689. [PubMed: 8840861]
38. Tseng Y, Kole TP, Wirtz D. Micromechanical mapping of live cells by multiple-particle-tracking microrheology. Biophys J. 2002; 83:3162–3176. [PubMed: 12496086]
39. Tzima E, del Pozo MA, Shattil SJ, Chien S, Schwartz MA. Activation of integrins in endothelial cells by fluid shear stress mediates Rho-dependent cytoskeletal alignment. EMBO J. 2001; 20:4639–4647. [PubMed: 11532928]
40. Tzima E, Irani-Tehrani M, Kiosses WB, Dejana E, Schultz DA, Engelhardt B, Cao G, DeLisser H, Schwartz MA. A mechanosensory complex that mediates the endothelial cell response to fluid shear stress. Nature. 2005; 437:426–431. [PubMed: 16163360]
41. Wang N, Butler JP, Ingber DE. Mechanotransduction across the cell surface and through the cytoskeleton. Science. 1993; 260:1124–1127. [PubMed: 7684161]
42. Xu J, Viasnoff V, Wirtz D. Compliance of actin filament networks measured by particle-tracking microrheology and diffusing wave spectroscopy. Rheologica Acta. 1998; 37:387–398.
43. Yamada S, Wirtz D, Kuo SC. Mechanics of living cells measured by laser tracking microrheology. Biophys J. 2000; 78:1736–1747. [PubMed: 10733956]
44. Yanai M, Butler JP, Suzuki T, Sasaki H, Higuchi H. Regional rheological differences in locomoting neutrophils. Am J Physiol Cell Physiol. 2004; 287:C603–C611. [PubMed: 15163623]

45. Yap B, Kamm RD. Mechanical deformation of neutrophils into narrow channels induces pseudopod projection and changes in biomechanical properties. J Appl Physiol. 2005; 98:1930–1939. [PubMed: 15640383]

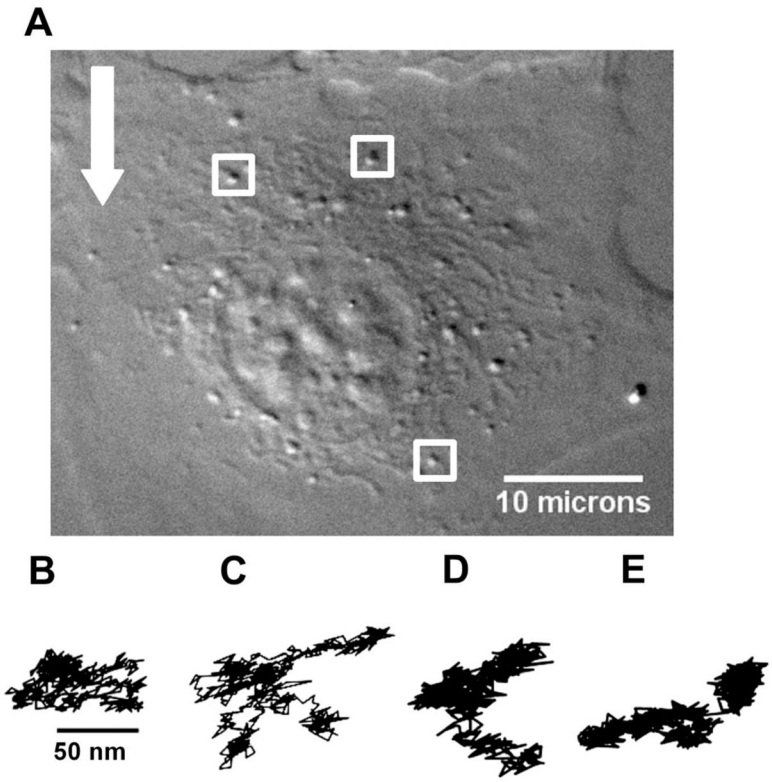

Fig. 1.

High-resolution imaging and tracking of endogenous vesicles in endothelial cells. *A*: bovine aortic endothelial cell (EC) imaged under high-resolution differential interference contrast microscopy. Endogenous vesicles (highlighted by white boxes) were tracked in a focal plane 2–4 μm from the base of the cell. Arrow indicates direction of fluid flow. Two-dimensional trajectories of endogenous vesicles calculated before step flow (preshear) was imposed (*B*), 30 s (*C*) and 4 min (*D*) after the onset of step flow (during shear), and 30 s after step flow was turned off (postshear; *E*).

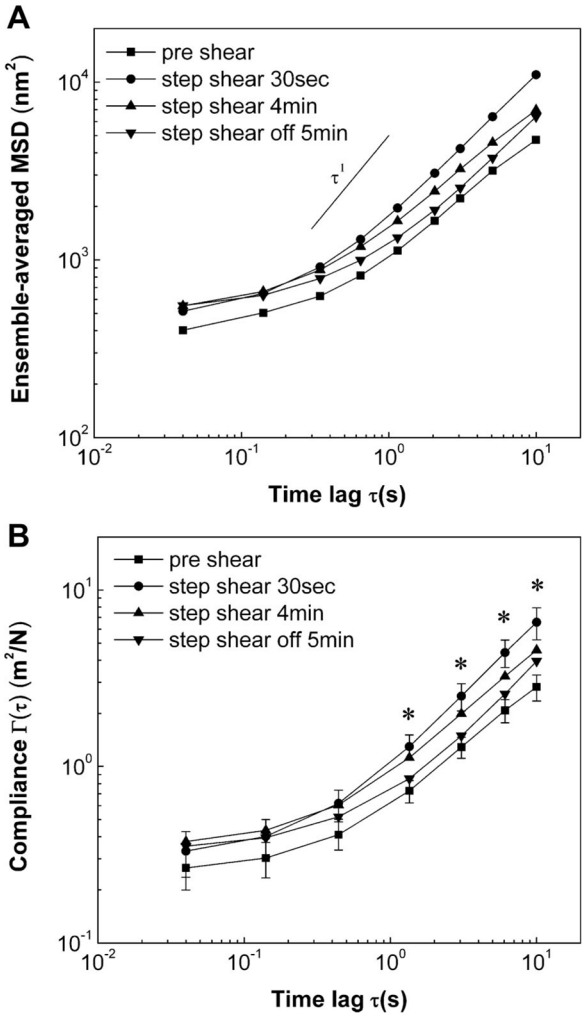

Fig. 2.

EC mechanics in response to step change in shear stress from 0 to 10 dyn/cm^2. *A*: ensemble-averaged mean square displacement (MSD) plotted against increasing time lags exhibits power-law scaling. $\alpha < 1$ indicates subdiffusive behavior of tracked endogenous vesicles. *B*: creep compliance curves of ECs for all experimental conditions. A twofold increase in creep compliance compared with preshear values was observed at very early time points (30 s) after onset of step shear stress. No change in creep compliance was observed when compared with initial static conditions, after shearing cells for 4 min, and after shear stress was removed in a stepwise manner. Data are means ± SE ($n = 6$). *$P < 0.05$ for 30 s step shear vs. static control preshear. Error bars for 4 min shear and 5 min postshear are not shown for clarity.

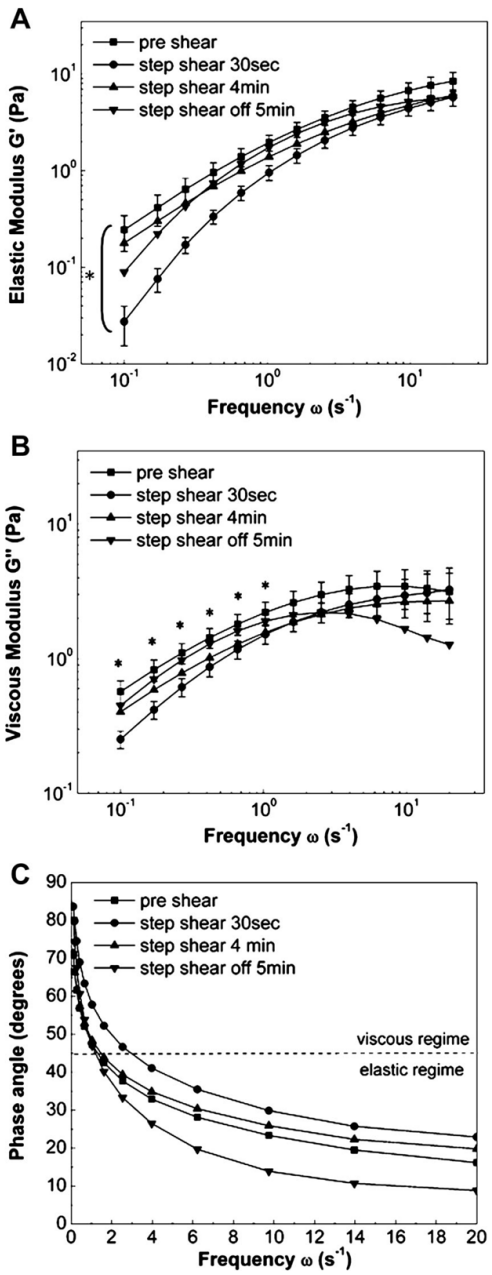

Fig. 3.

Shear-induced adaptive microrheology. Frequency-dependent elastic (*A*) and viscous (*B*) moduli decreased rapidly after exposure to step shear of 0 to 10 dyn/cm^2. After 4 min of shearing was completed, values returned to preshear levels. No change in rheology was seen after shear stress was removed. 1Pa = 10 dyn/cm^2. Data are means ± SE; $n = 6$. *Significant differences between preshear and 30 s shear rheological moduli ($P < 0.05$) at all frequencies (*A*) and for indicated frequencies (*B*). Error bars for 4 min shear and 5 min postshear are not shown for clarity. *C*: frequency-dependent viscoelastic phase angles indicate that ECs cross over from the viscous to the elastic regime at frequency of 1 s^{-1}. Imposition of step shear stress increases the crossover frequency to 3 s^{-1}.

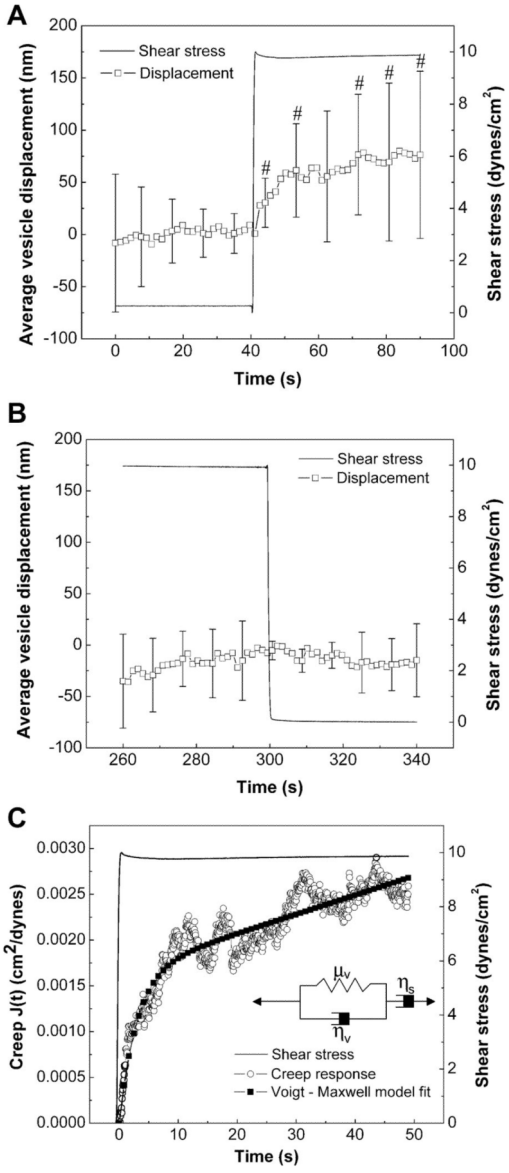

Fig. 4.

Macrorheology of endothelial cells. Heterogeneous global cell deformation measured from average vesicle displacements due to step change in shear stress. *A*: ECs exhibited time-dependent deformation when step shear stress was turned on (0 to 10 dyn/cm^2). #Significant displacements compared with 0 displacement using 95% confidence intervals. *B*: negligible cell deformation was seen upon removal of shear stress in a stepwise manner (10 to 0 dyn/cm^2). Data are means ± SD (n = 6). *C*: curve-fitting average creep response to a phenomenological model shows that ECs behave like viscoelastic liquids with a relaxation time of 3 s. *Inset*: Voigt-Maxwell model used to describe the creep response of ECs.